The reduced modulus in the analysis of sharp instrumented indentation tests

Sara A. Rodríguez[a)]
Research Group of Fatigue and Surfaces, Mechanical Engineering School, Universidad del Valle, Cll 13 No 100-00, Cali, Colombia; and Department of Mechanical Engineering, Surface Phenomena Laboratory, University of São Paulo, 2231 05508-900 São Paulo, Brazil

Jorge Alcalá
GRICCA-EUETIB, Universitat Politècnica de Catalunya, Barcelona 08036, Spain

Roberto M. Souza
Department of Mechanical Engineering, Surface Phenomena Laboratory, University of São Paulo, 2231 05508-900 São Paulo, Brazil

(Received 29 February 2012; accepted 30 April 2012)

In the analysis of instrumented indentation data, it is common practice to incorporate the combined moduli of the indenter (E_i) and the specimen (E) in the so-called reduced modulus (E_r) to account for indenter deformation. Although indenter systems with rigid or elastic tips are considered as equivalent if E_r is the same, the validity of this practice has been questioned over the years. The present work uses systematic finite element simulations to examine the role of the elastic deformation of the indenter tip in instrumented indentation measurements and the validity of the concept of the reduced modulus in conical and pyramidal (Berkovich) indentations. It is found that the apical angle increases as a result of the indenter deformation, which influences in the analysis of the results. Based upon the inaccuracies introduced by the reduced modulus approximation in the analysis of the unloading segment of instrumented indentation applied load (P)–penetration depth (δ) curves, a detailed examination is then conducted on the role of indenter deformation upon the dimensionless functions describing the loading stages of such curves. Consequences of the present results in the extraction of the uniaxial stress–strain characteristics of the indented material through such dimensional analyses are finally illustrated. It is found that large overestimations in the assessment of the strain hardening behavior result by neglecting tip compliance. Guidelines are given in the paper to reduce such overestimations.

I. INTRODUCTION

In recent years, instrumented indentation techniques have been increasingly used to determine the uniaxial mechanical properties of bulk materials and coatings through analytical and numerical solutions of the correlation between indentation load–displacement curves and such properties. Since the majority of these solutions are obtained for idealized *rigid* tips, some adjustments are required to account for the indenter deformation that occurs in actual experiments. This is commonly performed by recourse to the so-called reduced elastic modulus, as defined through Eq. (1) in Sec. II.[1–3] A fundamental assumption in the use of the reduced modulus is that two systems (Table I), one with a rigid indenter and the other with an elastic indenter, are equivalent as long as the reduced modulus is the same.

Instrumented indentation tests are carried out with systems in which the indentation load and the indenter tip displacement are continuously registered. At any load stage, the total displacement, as measured by the transducer, is the sum of the true indenter displacement below the original specimen surface and the displacement of the load train of the system (i.e., the system compliance). Upon correction of measured load–displacement curve for machine compliance,[1] the resulting curve shall ideally measure the correlation between the applied indentation load (P) and the distance of indenter–sample mutual approach (δ). It is well known from classic linear elastic contact mechanics[4] that δ is not the magnitude of the indenter penetration below the original surface of the elastic half-space (h_s) but the total displacement by which two remote points, one in the indenter and the other one in the half-space, approach each other. (Clarification is here needed in that while in our prior investigations, we use variable h_s to denote measured penetration depth from the free surface,[3,5] this is only so when dealing with *rigid* indenter tips.)

[a)]Address all correspondence to this author.
e-mail: sararopu@gmail.com
DOI: 10.1557/jmr.2012.164

 © Materials Research Society 2012

https://doi.org/10.1557/jmr.2012.164 Published online by Cambridge University Press

TABLE I. Elastic properties and contact parameters.

	System 1 (rigid indenter)	System 2 (elastic indenter)
Normal displacement of surface of indenter (u_{z1})	0	$u_{z1(2)}$
Normal displacement of surface of indented material (u_{z2})	$u_{z2(1)}$	$u_{z2(2)}$
Radial displacement of surface of indented material (u_r)	0	$u_{r(2)}$
Radius of contact (a)	$a_{(1)}$	$a_{(2)}$
Total load compressing the solids (P)	$P_{(1)}$	$P_{(2)}$
Distance of indenter–sample mutual approach (δ)	$\delta_{(1)}$	$\delta_{(2)}$
Indenter penetration below the original surface of the indented surface (h_s)	$h_{s(1)} = \delta_{(1)}$	$h_{s(2)}$
Elastic modulus of the indented material (E)	$E_{(1)}$	$E_{(2)}$
Poisson's ratio of the indented material (ν)	$\nu_{(1)}$	$\nu_{(2)}$
Elastic modulus of the indenter (E_i)	∞	E_i
Poisson's ratio of the indenter (ν_i)	0	ν_i
Reduced modulus (E_r)	$E/(1-\nu^2)$	$[(1-\nu^2)/E + (1-\nu_i^2/E_i)]^{-1}$

Some controversy has been raised on the validity of the reduced modulus assumption,[6–9] which evidently translates into the extraction of mechanical properties from indentation P–δ curves. In the case of conical indentation, a conclusion of the experimental study[7] was that the reduced modulus assumption led to serious inaccuracies in the case of contact loadings imposed by elastic (rubber) cones onto rigid half-spaces (soda–lime glass block) or onto materials whose elastic modulus is close to that of the indenter. In these limiting cases, better results were obtained by regarding the indenters as rigid than by recourse to the reduced modulus assumption. The experiments are somewhat unclear in the fact that the elasticity of the indented rubber may be nonlinear as well as concerning the role of friction on the overall behavior. Also, other experimental results[10] using tungsten carbide cones pressed against elastic blocks of both rubbers and different compositions of polydimethylsiloxane showed that with the exception of the penetration of a 60° cone, the indentation load–depth curves of all the elastic solids were well fitted by the so-called Sneddon's solution for frictionless indentations with ideally rigid tips. Attention is drawn to the fact that the experiments represent the behavior of an extremely rigid tip, so that they may not be applicable under the large elastic contrasts between indenter tip and material arising in the indentation of metals and ceramics. Additional investigations have further illustrated that the use of the reduced modulus for nonrigid indenter tips underestimates the curvature of the load–depth curve when indenting elastoplastic metals with diamond and sapphire Berkovich tips.[11]

Correction of the contact area has also been claimed to be necessary due to the deformation of the indenter during penetration.[8,12,13] This may affect in the calibration for the compliance of the indenter apparatus, which is commonly performed by estimating the contact area–δ function from instrumented indentation measurements.[14] In this sense, deviation of the determined area function from that of perfect indenter geometry has been previously attributed to indenter deformation during contact.[15] Although tip defects always exist, systematical analysis of indenter deformation effect on the area function determined by calibration is not available in the literature.

Assuming that the real contact area could be measured with precision, a correction is still necessary in Sneddon's equation to account for indenter tip deformation. An explicit expression for the elastic unloading of a conical indenter with half apex angle, $\theta = 70.3°$, has been presented as a function of the ratio E/E_i and the Poisson's ratio of the indenter material.[16]

This work provides a detailed analysis on the role of elastic indenter deformation in instrumented indentation measurements as well as on the validity of using of the reduced modulus assumption in its assessment. The investigation comprises finite element simulations for axisymmetric conical ($\theta = 70.3°$) and pyramidal Berkovich indenters. The analysis essentially concerns the shape of the P–δ curve obtained with nonrigid tips; the possible flattening of indenter tips during penetration and the impact of this upon the use of Sneddon's relation in three-dimensional (3D) pyramidal contacts; and the explicit influence of elastic indenter deformation in the dimensionless relations used to assess mechanical properties from instrumented indentation.

II. THEORETICAL BACKGROUND

The reduced modulus (E_r) emerges from the elastic contact analysis by Hertz:

$$\frac{1}{E_r} = \frac{(1-\nu^2)}{E} + \frac{(1-\nu_i^2)}{E_i} \quad , \qquad (1)$$

where E and E_i are the elastic moduli and ν and ν_i are the Poisson ratios of the material and the indenter, respectively. For the same value of E_r, identical P–δ curves are attained for both rigid and elastic indenters brought into contact against elastic solids irrespectively of the specific moduli of the indenter and the material. The analysis is obviously restricted to the approximations in the Hertzian

https://doi.org/10.1557/jmr.2012.164 Published online by Cambridge University Press

analysis, explicitly covering indenters and indented materials whose nonconforming frictionless contact behavior can be described through the linearized (small-strain) elasticity theory.[4]

In his analysis of the *elastic* indentation of a flat surface by a sharp rigid cone of half-apical angle, θ, Love[17] showed that the mean pressure (p_m) on the face of the cone, tip penetration (h_s), and applied force (P), respectively, are given by Eqs. (2)–(4).

$$p_m = \frac{1}{2}\frac{E}{1-\nu^2}\cot(\theta) \quad , \tag{2}$$

$$h_s = \pi p_m a \frac{1-\nu^2}{E} \quad , \tag{3}$$

$$P = \frac{1}{2}\pi a^2 \frac{E}{1-\nu^2}\cot(\theta) \quad . \tag{4}$$

Also following Sneddon's relation,[18] it is noted that

$$h_s = \frac{\pi h}{2} = \frac{\pi a}{2\tan\theta} \quad , \tag{5}$$

where h is the actual contact depth from the contact boundary (where material sinking-in occurs) to the center of the imprint. (It is noted that other nomenclature is also commonly used for this penetration depth, where $h = h_c$.) Since from Eqs. (4) and (5), h_s and P are related through

$$P = \frac{2}{\pi}\frac{E}{(1-\nu^2)}\tan(\theta)h_s^2 \quad . \tag{6}$$

Equations (5) and (6) allow finding of the indentation stiffness

$$S = \frac{2}{\sqrt{\pi}}\frac{E}{1-\nu^2}\sqrt{A} \quad , \tag{7}$$

where $S = dP/dh_s$ and A is the true projected contact area accounting for material pileup and sinking-in. Equation (7) is usually referred to as Sneddon's relation. Following these investigations, Eq. (7) has been extensively used in the analysis of the unloading (presumably elastic) stage from instrumented indentation experiments as in the landmark paper by Oliver and Pharr[1]; in this sense, a similar formulation can be traced to the work by Bulychev et al.[19]

The work by Hay et al.[20] is illustrative in showing that in addition to the vertical displacement (u_z) imposed by the indenter tip, inward (negative) radial displacements (u_r) are a concomitant to the above elastic analyses by Love and Sneddon. This is unrealistic because a true (physical) indenter cannot assimilate such inward displacements without restrain. Therefore, Hay et al.[20] find that for a fixed penetration depth, the actual indentation load for a rigid conical indenter shall be greater than that from the analytical solution because the occurrence of radial (inward) displacements in the material are prevented by the indenter body. The implicit lack of material containment in the analytical solution thus softens the P–h_s curve.

Furthermore, it is important to note that for elastic indenter tips, an increase in the original apex angle of the indenter is anticipated with increasing penetration, which is expected to lead to variations in the shape of P–δ curve.[7,9,16] Thus, considering the indentation configurations in Table I, $\theta_{(1)}$ must be lower than $\theta_{(2)}$ so that even in the assumption that $E_{r(1)} = E_{r(2)}$, the two configurations shall render different contact responses [Eq. (6)].

The reduced modulus concept is also used in reverse algorithms for extracting the material properties (i.e., the uniaxial stress–strain characteristics) of elastic–plastic materials from instrumented indentation loading and unloading curves.[2,3,21] These algorithms rely on dimensional analyses of the indentation behavior of elastic–power law plastic solids, where it is taken that for ideally self-similar sharp indentations,

$$P = f(\delta, E, \nu, Y, n, E_i, \nu_i) \quad , \tag{8}$$

where n is the power law hardening coefficient and Y as yield strength.[22] Equation (8) is then often simplified using the reduced modulus E_r,[2] so that

$$P = f(h_s, E_r, Y, n) \quad . \tag{9}$$

Various useful dimensionless, Π, functions derived on the basis of Eq. (9) are given in literature.[2,3,22] While this approach has been extensively investigated over the years, a systematic analysis remains unavailable to our knowledge on the influence of the reduced modulus assumption in such functions and on how this affects inferred mechanical properties.

III. FINITE ELEMENT ANALYSIS

Finite element simulations were carried out using the commercial code ABAQUS to model the indentation response of elastic and elastic–plastic solids. For conical indentation, a two-dimensional (2D) mesh of 2097 four-node axisymmetric elements of type CAX4R was used. For Berkovich indentation, a 3D mesh of 18,600 eight-node elements type C3D8R was used. The indenters were represented by a 2D mesh of 384 axisymmetric elements in the conical case, combining four-node type CAX4R and three-node type CAX3 elements. In the Berkovich case, the indenter was represented by a 3D mesh of 2416 eight-node elements type C3C8R. To eliminate the size effects induced by the distance to the boundary condition used in modeling the indenter tip, the indenter dimensions were increased maintaining the same geometry to a point where an additional increase did not produce measurable changes in the P–δ indentation curve.[16]

https://doi.org/10.1557/jmr.2012.164 Published online by Cambridge University Press

The indented material was modeled as a homogeneous and isotropic solid obeying the J_2-associated flow theory of plasticity with Poisson ratio ν fixed at 0.3. (The reader is directed to the work by Alcalá and Esque-de-los-Ojos,[23] for a detailed assessment of the validity of this theory in the modeling of indentation experiments in polycrystalline aggregates.) In these simulations, Y and n are defined through the following relation between the uniaxial stress σ and total uniaxial (elastic plus plastic) strain ε:

$$\varepsilon = \begin{cases} \sigma/E, & \text{for } \sigma < Y \\ \left(Y/E\right)\left(\sigma/Y\right)^{1/n}, & \text{elsewhere} \end{cases} . \quad (10)$$

Three combinations of elastic moduli (denoted as sets 1–3 in Table II) were used in the simulations, both for rigid (sets A in Table II) and elastic indenters (sets B in Table II). Additionally, solids with $E = 400$, 200, and 50 GPa were indented using a rigid tip for the sake of comparison with the results obtained for elastic indenters. Six levels of ratio E_r/Y (0, 10, 20, 100, 200, and 1000) for $n = 0$ were simulated for each of the six combinations of elastic properties shown in Table II, totaling 36 simulations for each indenter (it is noted that $E_r/Y = 0$ implies perfectly elastic indented material). For a better representation of metallic materials, additional simulations were performed for solids with two levels of power law strain hardening coefficient, n, = 0.25 and 0.5, using all elastic combinations in Table II at two levels of ratio $E_r/Y = 200$ and 2000. The elastic (diamond) indenter tips were assumed to have an elastic modulus E_i of 1029 GPa (Table II) and Poisson ratio ν_i of 0.07 (note that rigid indenters imply $E/E_i = 0$).

All simulations were performed for frictionless contacts at large strains and rotations. Such frictionless conditions were assumed by considering previous analyses, where it is found that while the amount of material pileup and sinking at the contact boundary is strongly affected by friction, the mechanical properties calculated from the P–h_s curves remain essentially unaffected.[21,23–25] The normal load was applied under displacement control. In all cases, a maximum displacement of 5 μm was imposed at the top of the indenter.

IV. RESULTS AND DISCUSSION

A. The role of indenter tip deformation in elastic instrumented indentations

Figure 1 presents the P–δ curves obtained using the finite element method for perfectly elastic materials ($E_r/Y = 0$). For conical and Berkovich indenters penetrating into elastic solids with identical reduced modulus, greater loads were obtained for rigid than for elastic indenters in good agreement with the conceptions in Sec. II. For instance, at fixed δ and identical reduced modulus $E_r = 308.4$ GPa, a load level 9% greater was applied by the rigid tip (see set 1A in Table II) than in the case of the elastic tip (see set 1B in Table II). Similar differences were obtained for $E_r = 181.3$ and 52.2 GPa, where the load increases ≈6% and 2%, respectively, for the rigid tip as compared to the elastic indenter case.

TABLE II. Elastic properties of indented materials and indenters.

Set	E (GPa)	E_i (GPa)	E_r (GPa)
1A	280.7	∞	308.4
1B	400	1029	308.4
2A	164.9	∞	181.3
2B	200	1029	181.3
3A	47.5	∞	52.2
3B	50	1029	52.2

In spite of the above results, it is remarked that much better agreement between the P–δ curves of elastic and rigid indenters was obtained when the reduced modulus [instead of the direct value of $E/(1 - \nu^2)$] is used to incorporate the deformation of the indenter. Results not shown in Fig. 2 indicated that the penetration of a *rigid* cone by 5 μm into a surface with $E = 400$ GPa required 55% more load than the case of the *elastic* cone (diamond) indenting the same surface. Similarly, greater loads by factors 28% and 7% are also required in the case of the indentation of materials whose elastic moduli are 200 and 50 GPa, respectively.

Analytical solutions are also presented in Fig. 1 [$\theta = 70.3°$ and E_r in the place of $E/(1 - \nu^2)$ in Eq. (6)]. Sneddon's solution allowing the inward (negative) displacement field u_r underestimates load as compared to the simulations for rigid indenters. In indentations performed with elastic indenters, radial displacement of the tip is possible depending on the elastic contrast E/E_i between indenter and material. Such a displacement then leads to changes in the apical angle. The present results show that for a fixed penetration of a *conical* indenter tip, the load applied by elastic indenters was underestimated [Fig. 1(c)] or overestimated [Fig. 1(a)] as compared to the analytical (Sneddon's) solution using the reduced modulus. Such over- and underestimations depended on ratio E/E_i as illustrated by these figures. Note that the analytical solution for a cone with half apex angle equal to 70.3° using E_r in the place of $E/(1 - \nu^2)$ underestimated the load for both elastic and rigid Berkovich indenters [see Figs. 1(a)–1(c)]. This is taken to illustrate the fact that the reduced modulus represents a mere approximation to a more complex problem. It is finally noted that the loads required to achieve the same penetration depth in these elastic materials are greater for Berkovich than for conical indenters.

Figure 2 illustrates the change in the shape and apex angle of elastic conical indenters pressed against elastic materials. In these indentation processes, the half apex angle of the cone varies from its original value of 70.3° to

https://doi.org/10.1557/jmr.2012.164 Published online by Cambridge University Press

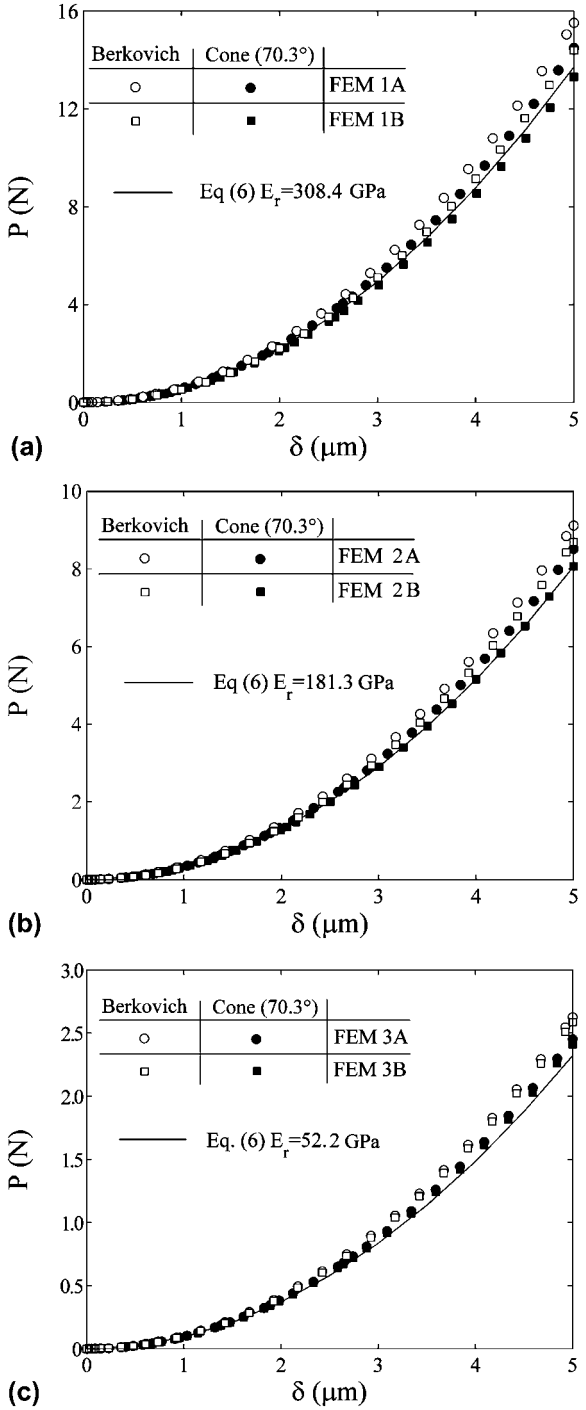


FIG. 1. Load–displacement curves predicted by finite element method with rigid and elastic conical and Bekovich indenters. Perfectly elastic indented materials with modulus (a) 1A and 1B; (b) 2A and 2B; and (c) 2A and 2C from Table II are illustrated in the figures.

84°, 80°, and 75° for the cases 1B, 2B, and 3B, respectively (Table II). While these apical angles are measured directly from the deformed indenter shapes in the simulations, a variation in the angle from the original value of 70.3°, which yields the same contact area–penetration

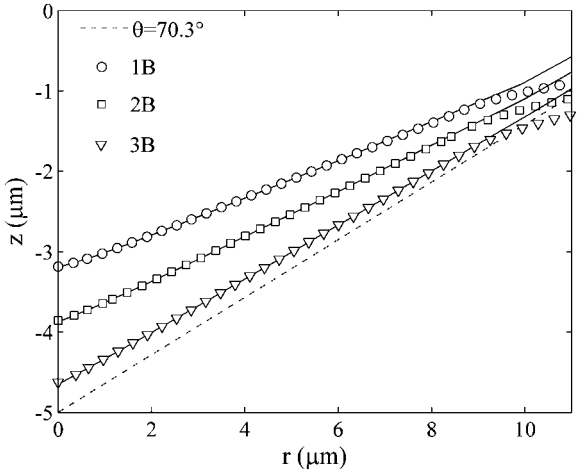


FIG. 2. Shape of the contact surface on maximum load of elastic materials from Table II when indented by elastic cone of 70.3°. Solid lines correspond to the deformed indenters shape and the doted line corresponds to an indenter with half apex angle equal to 70.3°.

depth function between the indenters, has been indirectly assessed from the variation in such function.[12,15] For instance, Troyon and Huang,[12] working with fused quartz, estimated that a cone with half apex angle of 74.6° is equivalent to a Berkovich indenter. These authors indicated that this variation over the original value of 70.3° was mainly due to the different flattening responses of the tips.

Recent works have shown that the exponent of the loading segment of the P–δ curves [Eq. (11)] deviates from 2 mainly as a result of the increase in indenter tip roundness.[26–28] By fitting the loading segments of the P–δ curves obtained in the finite element simulations to Kick's law

$$P = K\delta^{\lambda} \quad , \tag{11}$$

the mean value of λ obtained in conical and Berkovich indentations was 2.0077 ± 0.0011 and 2.0156 ± 0.0250, respectively. Note that since λ shall remain equal to 2 in Kick's law irrespectively of the apex angle of the tip (i.e., changes in tip angle would affect K but not λ), the presently found preservation of $\lambda \approx 2$ suggests that there would be no significant flattening or change in indenter *shape* during penetration.

B. The influence of indenter tip deformation in the variables ruling elastoplastic instrumented indentation

This section concerns evaluation of the influence of the elastic contrast E/E_i in the different dimensionless relations that have been previously used in the analysis of instrumented indentation under the assumption of self-similar contact responses (i.e., in the absence of indentation size effects). In what follows, we shall thus examine the influence of the reduced modulus approximation in a

https://doi.org/10.1557/jmr.2012.164 Published online by Cambridge University Press

selected set of dimensionless relations where the equivalency between Eqs. (8) and (9) is assumed. Then, the deviation from unity in the ratio between each such relations and their respective values for rigid tips ($E/E_i = 0$) is regarded as a measure of the inaccuracies introduced by the reduced modulus assumption.

We shall start the discussion by considering dimensionless relation $\Pi_1 = P/E_r\delta^2$,[2] which is shown in Fig. 3 for the elastic and elastic–perfectly plastic cases simulated in this work. [Note that in Fig. 3, the rigid indenter condition of $E/E_i = 0$ can be attained for the three different values of $E = 50$, 200, and 400 GPa used in this work as long as $E_i \to \infty$, so that in each of the data points located at $E/E_i = 0$ in Fig. 3(a), there are indeed three different overlapping simulations.] While this figure supports the practice of accounting for indenter deformation through the reduced modulus assumption at large values of $E_r/Y > 20$ (variation smaller than 3% in the dimensionless Π_1 relation with E/E_i), a deviation occurs as the elasticity of the material becomes more pronounced for $E_r/Y < 20$.

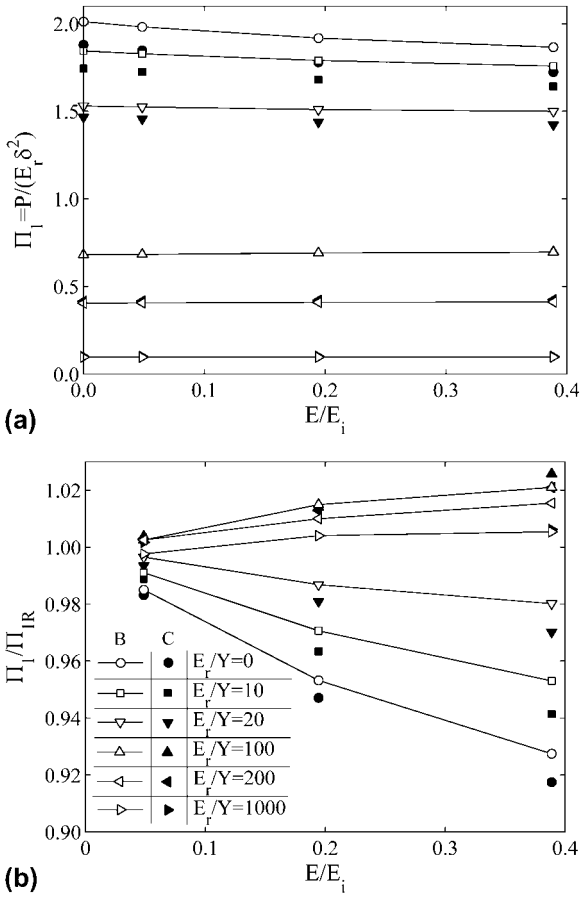


FIG. 3. (a) Variation of dimensionless load function Π_1 in elastic and elastic-perfectly plastic materials in terms of elastic contrast between indenter and material E/E_i. (b) Ratio between the dimensionless load function for elastic tips Π_1 and its equivalent for rigid tips Π_{1R}. B indicates Berkovich, and C indicates conical indenters.

Figure 3(b) presents the ratio Π_1/Π_{1R} between the values of the dimensionless relation Π_1 obtained with elastic indenters and the relation Π_{1R} for rigid indenters. For the elastic–perfectly plastic materials with ratio E_r/Y equal to 0, 10, and 20, Π_1 decreases when the ratio E/E_i increases. For the other materials, Π_1 increases when the ratio E/E_i increases. Strain hardening plays a role upon these results, as it increases the differences between elastic and rigid indenters. For instance, in the case of a material with $E_r/Y = 200$ and $n = 0$, Π_1/Π_{1R} reached 1.018 at $E/E_i = 0.39$, while, for the same E/E_i, Π_1/Π_{1R} reached 1.068 and 1.080 for $n = 0.25$ and $n = 0.5$, respectively.

For $E/E_i = 0$, the results in the literature already indicate that Π_1 decreases when the ratio E/Y increases.[2,5,22,27] Note that for a given E_r, ratio E/Y is lower in systems with rigid than with elastic indenter. (See Table III, where in systems whose $E_r = 308.4$ GPa, ratio E/Y of the indented material is up to 42% larger when indented by an elastic tip than with the rigid tip.) Moreover, the difference between the ratios E/Y for rigid and elastic tips decreases when the reduced modulus decreases. (This difference becomes up to 21% and 5.2% for $E_r = 181.3$ and 52.2 GPa, respectively, see Table III.) As consequence, Π_1/Π_{1R} shall be anticipated to be lower than 1 and decreases as the elastic contrast (E/E_i) increases because at constant E_r/Y, ratio E/Y still gradually increases. The results in Fig. 3(b) incidentally show that this explanation is indeed false for the large values of $E_r/Y > 100$, where Π_1/Π_{1R} *increases* with E/E_i.

The amount of pileup or sinking-in is quantified by parameter α, defined as the ratio between A and A_s (e.g., see Ref. 3):

$$A = \alpha A_s \quad . \tag{12}$$

In Eq. (12), A_s is the contact area as measured from the original surface (i.e., without pileup or sinking-in). In the absence of elastic deformation in the tip, this contact area A_s is thus identical to the cross-sectional area of the indenter at a depth equal to h_{max}. (It therefore strictly exists factor f so that $A_s = fh_s^2$. In the case of Berkovich indentation, $f = 25.56$.) Parameter α depends on the mechanical properties and is mainly influenced by n.[3]

Figure 4(a) gives the values of α calculated as the ratio between A, directly obtained from the finite element analysis, and A_s, calculated as $A_s = 25.56\,\delta_{max}^2$ (i.e., under the assumption that $\delta_{max} = h_{max}$, which is only strictly fulfilled for rigid tips, $E/E_i = 0$). Figure 4(b) shows α exhibiting the same behavior with E/E_i as function Π_1. A similar trend in terms of E/E_i, not shown in Fig. 4, was also obtained for materials that undergo strain hardening ($n \neq 0$), where α decreased up to 10% as E/E_i increases to the present limit of 0.39.

Accurate instrumented indentation testing relies on prior assessment of machine compliance. This is usually

https://doi.org/10.1557/jmr.2012.164 Published online by Cambridge University Press

TABLE III. Ratio between elastic modulus (E) and yield strength (Y) of the indented materials.

E_r (GPa)	E/E_i	E/Y (for $E_r/Y = 10$)	E/Y (for $E_r/Y = 20$)	E/Y (for $E_r/Y = 1009$	E/Y (for $E_r/Y = 200$)	E/Y (for $E_r/Y = 1000$)	E/Y (for $E_r/Y = 2000$)
308.4	0	9.10	18.20	91.00	182.00	910.00	1820.00
	0.39	12.70	25.94	129.68	259.36	1296.82	2593.64
181.3	0	9.10	18.20	91.00	182.00	910.00	1820.00
	0.19	11.03	22.07	110.34	220.68	1103.41	2206.82
52.2	0	9.10	18.20	91.00	182.00	910.00	1820.00
	0.05	9.58	19.17	95.83	191.67	958.35	1916.70

performed by finding the actual correlation between area A_s and penetration depth measurements δ_{max}. The resulting function is then used as a replacement for the ideal geometrical function, i.e., $A_s = 25.56\ \delta^2_{max}$ in the case of rigid Berkovich indentation where $h_s = \delta_{max}$. Usually, the $A_s - \delta_{max}$ function in solids undergoing sinking-in is obtained by assuming the following correlation.[29,30]

$$h = \delta_{max} - \varepsilon \frac{P_{max}}{S} \quad , \tag{13}$$

where ε is a geometrical factor that varies depending on m—the exponent of the unloading curve[29]; and S is the contact stiffness allowing contact area estimates under the assumption of Sneddon's relation with reduced modulus E_r. Because of the inaccuracy in the reduced modulus assumption described above, it is found that the use of Eq. (13) leads to errors of about 10% in the estimation of the contact area even in elastic–plastic materials presenting sinking-in ($E/E_i = 0.39$). This error adds to the uncertainties of the procedure, where a fixed value of ε needs to be further assumed in Eq. (13) where the value of ε used in the present analysis strictly adheres to its dependency with m—the exponent of the unloading curve—as originally described in Oliver and Pharr.[29]

Another dimensionless relation that has been adopted in the analysis of instrumented indentation data is $\Pi_2 = H/E_r$,[2,3,21,22,31] where H is the hardness defined as $H = P/A$ (Fig. 5). Figure 5(b) shows that the differences between Π_2 and Π_{2R} were smaller than 6% for the indentation of elastic–perfectly plastic materials. The effect of E/E_i on Π_2 was more pronounced in work-hardening materials, so that for instance, the value of Π_2/Π_{2R} reached 1.19 for $E_r/Y = 200$, $n = 0.5$ at $E/E_i = 0.39$.

Dimensionless parameters δ_e/δ_{max} and δ_r/δ_{max} characterize the unloading instrumented indentation stage, where δ_e is the intersection with $P = 0$ of a straight line of slope S drawn from point (P_{max}, δ_{max}), and δ_r is the residual indentation depth measured upon complete unloading.[2,3,21] Ratio δ_e/δ_{max} exhibited a slight variation, smaller than 5%, with ratio E/E_i for both conical and Berkovich indenters. Nevertheless, ratio δ_r/δ_{max} was extremely sensitive to the elastic contrast, decreasing by 17% when the ratio E/E_i was increased to 0.39 (Fig. 6). This variation in

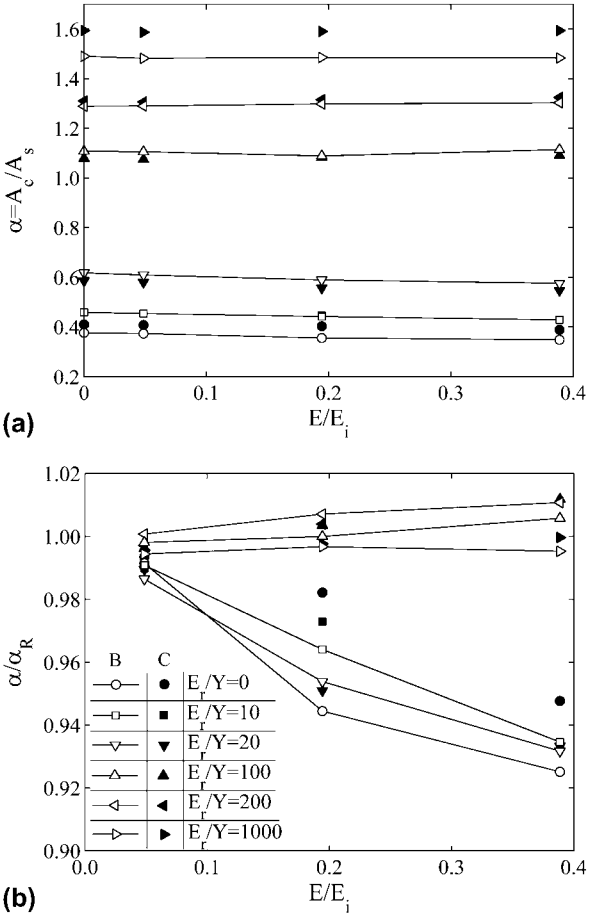


FIG. 4. (a) Quantification of the levels of pileup and sinking-in from parameter α obtained from the finite element simulations with elastic and elastic-perfectly plastic materials indented by conical (C) and Berkovich (B) indenters as a function of ratio E/E_i. (b) Ratio α/α_R for elastic and rigid indenters.

δ_r/δ_{max} can be explained because part of the elastic recovery during unload corresponds to the recovery of original indenter shape. The effect of E/E_i on δ_r/δ_{max} is thus anticipated to have important consequences in the assessment of the mechanical properties from algorithms based on the energy released during unloading.[32]

From the unloading indentation curve, the elastic modulus is usually estimated using the Sneddon's equation

https://doi.org/10.1557/jmr.2012.164 Published online by Cambridge University Press

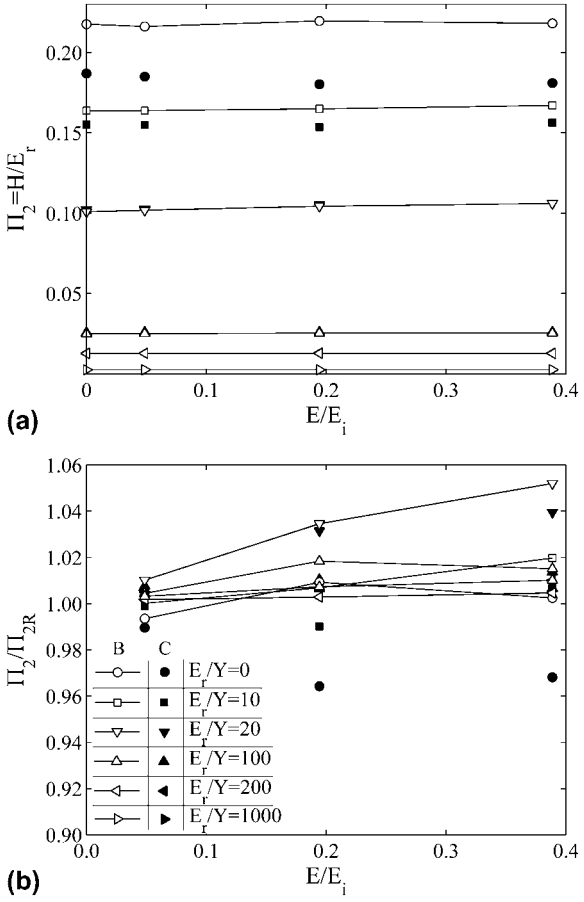


FIG. 5. (a) Dimensionless function $\Pi_2 = H/E_r$ in elastic and elastic-perfectly plastic indented materials as a function of E/E_i. (b) Ratio between dimensionless function for elastic tips Π_2 and its equivalent for rigid tips Π_{2R}. B indicates Berkovich, and C indicates conical indenters.

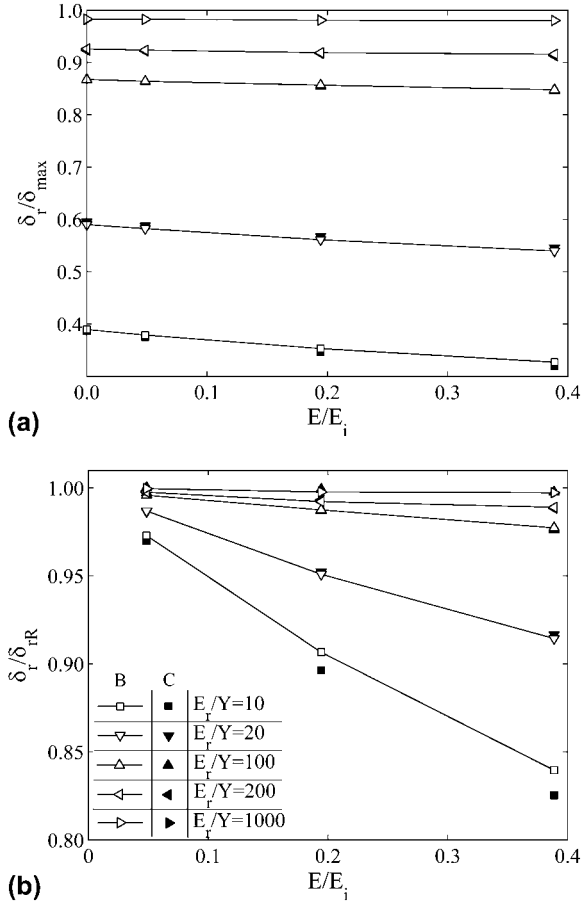


FIG. 6. (a) Relationships between δ_r/δ_{max} and ratio E/E_i in elastic and elastic-perfectly plastic materials. (b) Ratio between the residual indentation depth for elastic tips δ_r and its equivalent for rigid tips δ_{rR}. B indicates Berkovich, and C indicates conical indenters.

[Eq. (7)], where $E/(1-\nu^2)$ is replaced by the reduced modulus E_r and correction factor β is incorporated, as in

$$S = \frac{P_{max}/\delta_{max}}{1-\delta_e/\delta_{max}} = \beta\frac{2}{\sqrt{\pi}}E_r\sqrt{A} \quad . \qquad (14)$$

Correction factor (β) has been reported to dependent on (i) indenter geometry and Poisson's coefficient,[12,16,20,33] (ii) the level of pileup or sinking-in in case of Berkovich and Vickers indenters,[27,34] and (iii) the indenter elastic deformation in case of super-hard materials.[16] Influences of elastic anisotropy of an indented single crystalline unit of material upon the unloading (elastic) indentation behavior [Eq. (14)] measured with Berkovich indenters have also been covered in our recent works.[35,36]

Although ratio δ_e/δ_{max} was rather constant with elastic contrast E/E_i, use of the reduced modulus in Eq. (14) is an implicit approximation that leads to errors in this equation. These errors can be analyzed by assuming that β varies with E/E_i. Hence, by imputing direct values of P_{max}, δ_{max}, δ_e/δ_{max}, E_r, and A from the present simulations into Eq. (14), it then becomes possible to evaluate the influence of elastic contrast E/E_i on β [Fig. 7(a)]. In the case of conical indentation, where the contact area is circular, the correction factor was independent of the mechanical properties of the material and thus remained unaffected by changes in hardness. In this case, β varied 8.2% within the current range of E/E_i analyzed in this work. For Berkovich indenters, β depends on the level of pileup or sinking-in and thus becomes affected by the mechanical properties (i.e., ratio E_r/Y) as described in Ref. 5. In this case [Fig. 7(a)], we evaluate the value of β at $E/E_i = 0$ for the different elastic–perfectly plastic materials and proceed with its assessment by increasing E/E_i to the maximum value of 0.39. In addition to the variation in β induced by a change in mechanical properties, it is currently found that E/E_i introduces and additional decrease in β, which does not exceed 7%. Figure 7(b) finally shows that the relative change in β with respect to the value corresponding to rigid indenters, i.e., ratio β/β_R, with increasing E/E_i is essentially the same for Berkovich and conical indentations.

https://doi.org/10.1557/jmr.2012.164 Published online by Cambridge University Press

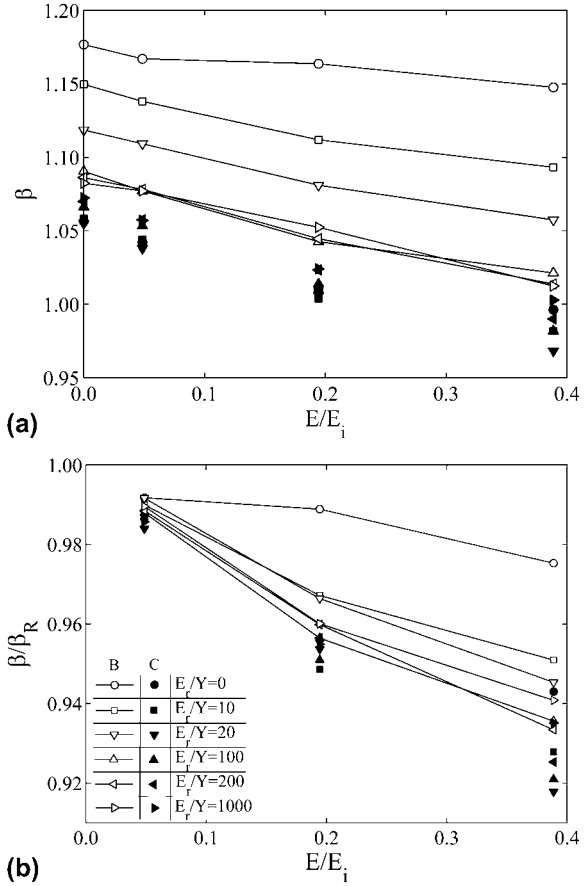


FIG. 7. (a) Correction factor β in terms of ratio E/E_i. (b) Ratio between correction factor for elastic tips β and its equivalent for rigid tips β_R. B indicates Berkovich, and C indicates conical indenters.

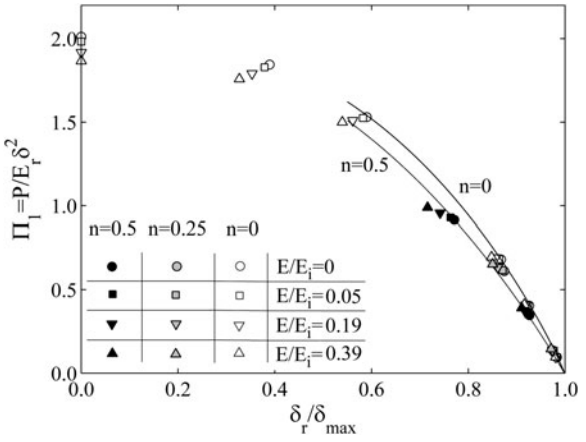


FIG. 8. Scaling dimensionless relationships between $\Pi_1 = P/E_r\delta^2$ and δ_r/δ_{max}. Binding curves are provided for the relationship between Π_1 and h_r/h_{max} for a rigid Berkovich indenter pressed against solids with hardening coefficient $n = 0$ and 0.5 from our previous investigation.[5]

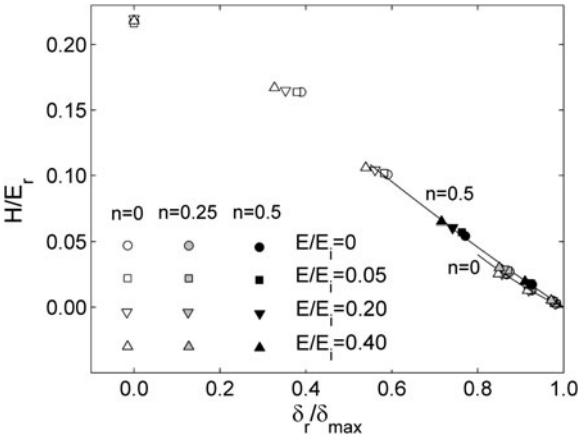


FIG. 9. Scaling dimensionless relationships between $\Pi_2 = H/E_r$ and δ_r/δ_{max}. Binding curves are provided for the relationship between Π_2 and h_r/h_{max} for a rigid Berkovich indenter pressed against solids with hardening coefficient $n = 0$ and 0.5 from our previous investigation.[3]

C. Quantification of the influence of indenter tip deformation in the dimensionless functions ruling instrumented indentation and in the extraction of the uniaxial stress–strain characteristics

Parametric relationships between dimensionless functions have been proposed to extract mechanical properties from indentation data.[2,3,21,27,31] Relationships between $\Pi_1 = P/E_r\delta^2$ and δ_r/δ_{max}, $\Pi_2 = H/E_r$ and δ_r/δ_{max}, and δ_e/δ_{max} and δ_r/δ_{max} are presented in Figs. 8, 9, and 10, respectively, for materials with different strain hardening responses. Another relationship between the dimensionless functions $K/\sigma_{0.033}$ and $E_r/\sigma_{0.033}$ is useful in the extraction of yield strength,[2,3] where $\sigma_{0.033}$ is an ad hoc representative stress level.

Figures 8–10 show that the variations of the dimensionless functions induced by the increment in E/E_i are equivalent to those that result when the value of hardening coefficient n is changed in indentations using rigid indenters ($E/E_i = 0$). This would obviously affect in any methodology where the computation of n is sustained upon dimensionless functions for rigid tips. Incidentally, this is an important difference with respect to spherical indentations, where, although the shape of the indentation curve changes with the increase in E/E_i, parametric relations between the dimensionless functions Π_1 and Π_2 and the ratio δ_r/δ_{max} are maintained for rigid and elastic indenters if E_r is used to account for indenter deformation.[37]

From the relationship between $K/\sigma_{0.033}$ and $E_r/\sigma_{0.033}$ (Fig. 11), which is hopefully independent of n,[2,3] the changes induced in K because of variations in elastic contrast E/E_i may readily lead to a change in the estimated representative stress $\sigma_{0.033}$.

Figure 10 presents the relationship between ratios δ_e/δ_{max} and δ_r/δ_{max}, which is well known to spread in terms of n.[3,5,21] In Fig. 10, continuous curves for $E/E_i = 0$ at $n = 0$ and for $E/E_i = 0$ at $n = 0.5$ are provided as bounds for the present computations through the dimensionless

https://doi.org/10.1557/jmr.2012.164 Published online by Cambridge University Press

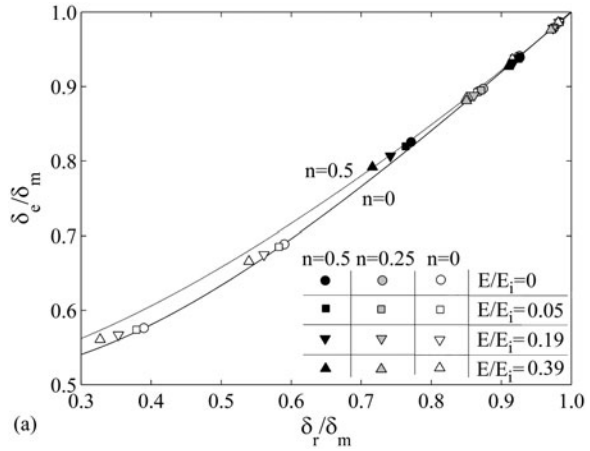


FIG. 10. Scaling dimensionless relationships between δ_e/δ_{max} and δ_r/δ_{max} for Berkovich indentation. The continuous binding curves for hardening coefficient $n = 0$ and 0.5 are for the *rigid* Berkovich indenter from our previous investigation.[5]

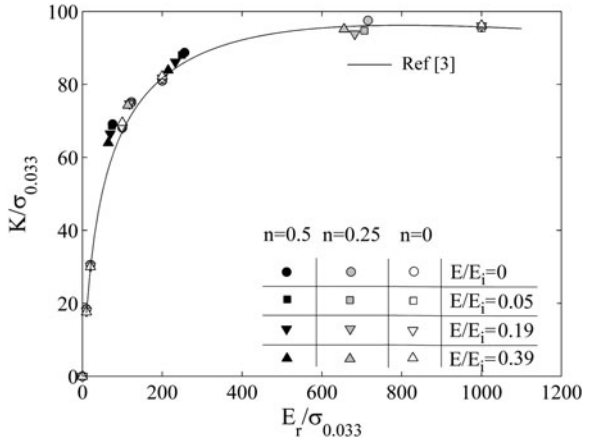


FIG. 11. Scaling dimensionless relationship between $K/\sigma_{0.033}$ and $E_r/\sigma_{0.033}$. The continuous curve corresponds to the rigid conical tip ($\theta = 70.3°$) used in Ref. 2.

function found in our recent work.[5] The correlation between the two penetration depth ratios and n has been demonstrated to be key in mechanical property assessments, as measurements of δ_e/δ_{max} and δ_r/δ_{max} from the P–δ curve permit calculation of hardening coefficient n.[5] In this context, the present simulations for different elastic contrasts between indenter and material show that the variation induced in both δ_e/δ_{max} and δ_r/δ_{max} because of indenter deformation does not modify the conclusion in our prior work in that materials whose δ_r/δ_{max} is greater than 0.7 exhibit a fundamental lack of uniqueness in mechanical property extractions. Hence, a given experiment providing one set of values for δ_e/δ_{max} and δ_r/δ_{max} can be regarded to have more than one possible solutions for n. (As described in our investigations, this duality can be resolved through direct measurement of the contact area, see Refs. 3, 5, 21, and 38.)

In spite of the ongoing discussion, indenter tip deformation leads to a sufficient variation in the relationship between δ_e/δ_{max} and δ_r/δ_{max} so as to significantly affect upon the inferred value of n. In this context, in a perfectly plastic material, this relationship shifted from the anticipated curve at $n = 0$ to that corresponding to $n = 0.5$ when ratio E/E_i increased. This effect is more pronounced in materials exhibiting large ratios of δ_r/δ_{max}, where a slight difference in the values of δ_e/δ_{max} and δ_r/δ_{max} leads to extreme variations in the inferred n.[3,5,21,39]

For the sake of illustration (Fig. 10), when ratio δ_r/δ_{max} is measured as 0.86 for a perfectly plastic material ($n = 0$, $E_r/Y = 100$, $E = 400$ GPa at $E/E_i = 0.39$), hardening coefficient is overestimated in 0.55 using the dimensionless function for rigid indenters that has been used in all our prior analyses. Keeping $\delta_r/\delta_{max} = 0.86$ as in the above, application of the dimensionless function obtained for rigid tips ($E/E_i = 0$) to a perfectly plastic material with $n = 0$ and $E = 200$ GPa ($E/E_i = 0.19$) yields hardening coefficient n of 0.42. Finally, when the same operation is performed for a material with 50 GPa ($\delta_r/\delta_{max} = 0.86$ and $E/E_i = 0.05$), n is estimated to be 0.34. By lowering ratio δ_r/δ_{max} to 0.75 ($E_r/Y = 200$, $n = 0.5$), the absolute error in n decreases to 0.091, 0.047, and 0.041 for the same respective values of $E/E_i = 0.39$, 0.19, and 0.05 as discussed above. The latter errors for $\delta_r/\delta_{max} = 0.75$ can be essentially neglected when compared to the influence of the experimental scatter in the inferred n.[5] Such errors are also comparable to the underestimation in n by 0.1, which has been anticipated to occur when neglecting frictional effects between indenter and material.[5,24,25] Incidentally, the aforementioned results provide a clear-cut explanation for our recent experimental evaluation of strong overestimations in n from our methodology for mechanical property extractions.[5]

In view of the current results, a sensible future line of work concerns finding of various dimensionless functions between δ_e/δ_{max} and δ_r/δ_{max} at different values of elastic contrast E/E_i. In the assumption that these functions were available, one could thus simple use the Oliver and Pharr approximation[29] to obtain a rough estimate of E. This will provide the value of E/E_i that is pertinent to the experiments at hand and allows use of the actual correlation between δ_e/δ_{max} and δ_r/δ_{max} ruling the experiment. In the current absence of these dimensionless functions, one can obtain an approximation of n by examining first the experimentally obtained value of δ_r/δ_{max}. If this ratio is smaller than, say, 0.82, one can simply take the rigid indenter solution ($E/E_i = 0$) for the correlation between δ_e/δ_{max} and δ_r/δ_{max} and extract the n value through the explicit formulations given in Refs. 5, 21, and 34. If $\delta_r/\delta_{max} > 0.80$, one can roughly decrease the inferred n under the above rigid indenter assumption by an amount of 0.35–0.40.

https://doi.org/10.1557/jmr.2012.164 Published online by Cambridge University Press

Another issue under investigation concerns extraction of yield strength from the dimensionless relationship between the ratios $K/\sigma_{0.033}$ and $E_r/\sigma_{0.033}$ in Fig. 11 and in the relationship between the ratios δ_r/δ_{max} and Y/E_r in Fig. 12. For a fixed value of hardening coefficient, the variation in ratio δ_r/δ_{max} because of indenter deformation is found to lead to an overestimation of the yield strength. For instance, for fixed values of E_r and n, use of the relationship between ratios δ_r/δ_{max} and Y/E_r translated into an overestimation of yield strength by 5% for $E/E_i = 0.05$, by 13% for $E/E_i = 0.19$, and by 22% for $E/E_i = 0.39$ (Fig. 12). These are relatively minor errors when compared to those introduced by experimental scatter[5] because in metals and ceramics, E/E_i is usually smaller than 0.17.

The relationship between $\Pi_2 = H/E_r$ and δ_r/δ_{max} is presented in Fig. 9. While preliminary investigations suggested that a single unique relation develops between these two parameters,[2,31] more recent studies show that the correlation splits in terms of n.[3] The results in Fig. 9 indicate that the influence of E/E_i upon Π_2 is rather mild as compared to that introduced into other dimensionless functions.

The level of pileup or sinking-in (as given by parameter α) has been prescribed in terms of h_r/h_{max} and hardening coefficient n.[3] Knowledge of α is crucial in contact area assessments so that its accurate measurement thus affects in further estimations of hardness and elastic modulus. Even if n is known a priori, the decrease of the ratio δ_r/δ_{max} induced at increasing elastic contrasts E/E_i leads to an underestimation of the contact area. This is because of the known increase in α with increasing h_r/h_{max}.[3]

D. Comparison between the indentation response of pyramidal and conical tips

The indentation behavior measured with pyramidal Berkovich and Vickers indenters has been usually approximated to that of a conical indenter with a half apex angle θ equal to 70.3° because the latter gives the same depth to area relationship as the above pyramids. Indentations with Berkovich tips have been found to be either more rigid or less rigid than those with conical indenters[40,41] depending on the mechanical properties of the indented material. Our previous findings[3] also illustrated on the above assumption on the equality between conical and pyramidal indentations by considering the influence of conical, Berkovich, and Vickers indenters in the dimensionless functions ruling the indentation process. As shown in Figs. 3–8 at increasing E/E_i, the differences between the equivalent conical indenter and the Berkovich indenter increase. For the same properties of indented material ($E/E_i = 0$), the indenter load was smaller, up to 7.1%, for the cone than for the Berkovich indenter. The differences further increase, up to 8.2%, for elastic indenters.

For elastic materials indented by rigid tips, the contact area was 8% greater for conical than for Berkovich indenters. The differences in contact areas increase up to about 10% for the elastic indenters. In elastic–plastic material responses, larger contact areas were obtained for the Berkovich indenter as compared to the conical tip. The largest differences were of about 5% for $E_r/Y = 1000$.

The difference between the unloading dimensionless function δ_r/δ_{max} versus δ_e/δ_{max} for conical and Berkovich indenters was of about 2% for $E/E_i = 0$. This difference increases up to about 3% as the elastic contrast between indenter and material, E/E_i, increases to the present upper limit of 0.39. It is recalled that these variations introduced large uncertainties in the estimated n value (Sec. IV. C).

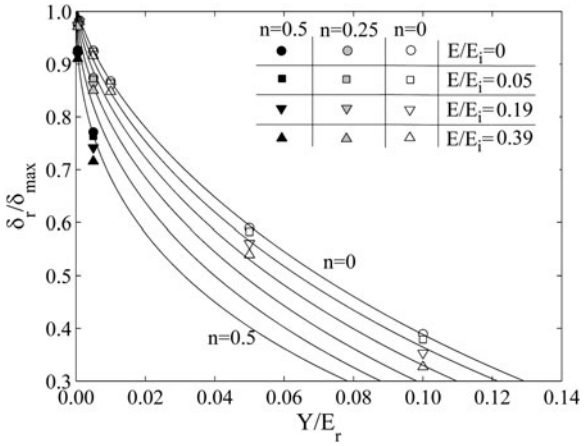


FIG. 12. Scaling dimensionless relationships between δ_r/δ_{max} and Y/E_r. The continuous curves correspond to the five relationships between h_r/h_{max} and Y/E_r for *rigid* Berkovich indenters where hardening coefficient n is varied from 0 to 0.5.[34]

V. CONCLUDING REMARKS

This investigation has provided a systematic assessment of the influence of indenter tip compliance on the analysis of the P–δ curves obtained through instrumented indentation experiments. In doing so, extensive finite element simulations have been performed where the elastic contrast E/E_i between indenter and material is varied from 0 (perfectly rigid indenter) to 0.05, to 0.19, and to 0.39. The analysis is performed for elastic and rigid materials exhibiting perfect plasticity (as given by strain hardening parameter $n = 0$) as well as marked power law strain hardening ($n > 0$). The above ranges of mechanical properties are assumed as they represent the response of essentially all metals and ceramics indented by diamond tips. The following are the main findings from the investigation.

(i) The so-called Sneddon's relation [Eq. (14)], which is conventionally used in the extraction of the elastic modulus of the material E from instrumented indentation unloading data requires correction for indenter tip compliance. This is so even when the reduced modulus E_r is used in Eq. (14) to account for the mutual elastic response

https://doi.org/10.1557/jmr.2012.164 Published online by Cambridge University Press

of indenter/material system [Eq. (1)]. Correction to Sneddon's relation is herein performed by assuming dependency of factor β in Eq. (14) to indenter tip deformations. It is found that β decreases with E/E_i to a maximum of 8.2% (Fig. 7). This variation needs to be taken into account when indenting elastically stiff solids such as some crystalline ceramics as alumina, whose E is in the range of 400 GPa ($E/E_i \sim 0.35$). It is noted that since both conical and Berkovich tips are modeled in this work, the above variation in β already incorporates the possible changes in this parameter because of the prevailing framework where pyramidal tips are approximated by the "equivalent" conical geometries for which Eq. (7) was indeed derived.

(ii) The deformation of conical and pyramidal (Berkovich) indenters during contact is amenable to analysis through a correction of the half-apical angle from the original undeformed value (i.e., $\theta = 70.3°$ for the conical tip). It is thus found that tip flattening—a hypothetical mechanism by which indenters may be assumed to change shape during contact—plays a negligible role upon the indentation behavior. The maximum variation estimated in tip angle involves change from $\theta = 70.3°$ to 84°.

(iii) A detailed analysis has been performed on the influence of indenter tip deformation on key dimensionless relations ruling instrumented indentation experiments. In this context, it is found that the reduced modulus approximation leads to significant alterations in such relations. It is therefore explicitly shown that while this practice is better than neglecting indenter tip deformations, it is far from being accurate.

(iv) Indenter tip compliance is also shown to play a key role in the extraction of the uniaxial stress–strain characteristics of the indented material. In this sense, it is found that the ratio between the residual indentation depth upon complete unloading and the maximum indenter displacement δ_r/δ_{max} decreases to an utmost value of 17% when compared to that exhibited by ideally rigid tips. This aspect in conjunction with the aforementioned inaccuracies introduced by the reduced modulus approximation leads to an overestimation of hardening coefficient n of, say, 0.3–0.4 for $\delta_r/\delta_{max} > 0.80$. That is to say that in perfectly plastic solids ($n = 0$), the extracted n value can be as large as 0.40. The influence of indenter tip compliance in the extraction of n can be however neglected when the indented material exhibits $\delta_r/\delta_{max} < 0.80$. Experimental support to these findings is given in our recent work,[5] where significant overestimations are found when n is inferred from instrumented indentations. Guidelines and possible research lines are discussed in the paper to minimize the influence of indenter deformation in such mechanical property extractions.

(v) Contact area estimates are usually used in the calibration of indenter systems to account for machine compliance. Interestingly, it is found that the contact area estimated by neglecting indenter tip compliance [Eq. (12)] may be significantly affected by this assumption, especially when elastically stiff solids are used in the calibration. The present work interestingly calls for the complementary use of soft and elastically compliant materials exhibiting sinking-in effects (such as well-annealed copper single crystals of high purity) when performing calibration of machine compliance to ensure that the results are not affected by indenter tip deformations. In doing so, our previous analyses of single crystal indentations with Berkovich tips may be instrumental in finding the equivalent value of E of the indented single crystal (e.g., Ref. 36). It is finally noticed that the increase in elastic contrast E/E_i enhances the differences between the indentation responses measured with actual pyramidal (Berkovich) indenters and their conical equivalent.

ACKNOWLEDGMENTS

This research was sponsored by the CNPq under Contract No. 141259/2007-8 and by the Spanish Ministry of Education and Science through Project MAT2008-01647/MAT.

REFERENCES

1. W.C. Oliver and G.M. Pharr: An improved technique for determining hardness and elastic modulus using load and sensing indentation experiments. *J. Mater. Res.* **7**, 1564 (1992).
2. M. Dao, N. Chollacoop, K.J. Van Vliet, T.A. Venkatesh, and S. Suresh: Computational modeling of the forward and reverse problems in instrumented sharp indentation. *Acta Mater.* **49**, 3899 (2001).
3. O. Casals and J. Alcalá: The duality in mechanical property extractions from Vickers and Berkovich instrumented indentation experiments. *Acta Mater.* **53**, 3545 (2005).
4. K.L. Johnson: *Contact Mechanics* (Cambridge University Press, Cambridge, 1985).
5. S.A. Rodríguez, R.M. Souza, and J. Alcalá: A critical reassessment of the elastic unloading in sharp instrumented indentation experiments: Mechanical properties extraction. *Philos. Mag.* **91**, 1409 (2011).
6. M.M. Chaudhri: A note on a common mistake in the analysis of nanoindentation data. *J. Mater. Res.* **16**, 336 (2001).
7. Y.Y. Lim and M.M. Chaudhri: Experimental investigations of the normal loading of elastic spherical and conical indenters on to elastic flats. *Philos. Mag.* **83**, 3427 (2003).
8. S.M. Jeong and H.L. Lee: Finite element analysis of the tip deformation effect on nanoindentation hardness. *Thin Solid Films* **492**, 173–179 (2005).
9. A.C. Ficher-Cripps: Use of combined elastic modulus in depth-sensing indentation with a conical indenter. *J. Mater. Res.* **18**, 1043–1045 (2003).
10. Y.Y. Lim and M.M. Chaudhri: Indentation of elastic solids with rigid cones. *Philos. Mag.* **84**, 2877–2903 (2004).
11. I. Choi, O. Kraft, and R. Schwaiger: Validity of the reduced modulus concept to describe indentation loading response for elastoplastic materials with sharp indenters. *J. Mater. Res.* **24**, 998–1006 (2009).
12. M. Troyon and L.Y. Huang: Correction factor for contact area in nanoindentation measurements. *J. Mater. Res.* **20**, 610–617 (2005).

https://doi.org/10.1557/jmr.2012.164 Published online by Cambridge University Press

13. M.G.J. Veprek-Heijman, R.G. Veprek, A.S. Argon, D.M. Parks, and S. Veprek: Non-linear finite element constitutive modeling of indentation into super- and ultrahard materials: The plastic deformation of the diamond tip and the ratio of hardness to tensile yield strength of super- and ultrahard nanocomposites. *Surf. Coat. Technol.* **203**, 3385–3391 (2009).
14. K.W. McElhaney, J.J. Vlassak, and W.D. Nix: Determination of indenter tip geometry and indentation contact area for depth-sensing indentation experiments. *J. Mater. Res.* **13**, 1300–1306 (1998).
15. J. Gong, H. Miao, and Z. Peng: On the contact area for nano-indentation tests with Berkovich indenter: Case study on soda-lime glass. *Mater. Lett.* **58**, 1349–1353 (2004).
16. Y.P. Cao, M. Dao, and J. Lu: A precise correcting method for the study of the superhard material using nanoindentation tests. *J. Mater. Res.* **22**, 1255–1264 (2007).
17. A.E.H. Love: Boussinesq's problem for a rigid cone. *Q. J. Math.* **10**, 161–175 (1939).
18. I.N. Sneddon: The relation between load and penetration in the axisymmetric boussinesq problem for a punch of arbitrary profile. *Int. J. Eng. Sci.* **3**, 47–57 (1965).
19. S.I. Bulychev, V.P. Alekhin, M.Kh. Shorshorov, A.P. Ternovskii, and G.D. Shnyrev: Determining Young's modulus from the indenter penetration diagram. *Ind. Lab.*, **41**, 1409–1412 (1975).
20. J.C. Hay, A. Bolshakov, and G.M. Pharr: A critical examination of the fundamental relations used in the analysis of nanoindentation data. *J. Mater. Res.* **14**, 2296–2305 (1999).
21. S.A. Rodríguez, M.C. Farias, and R.M. Souza: Finite element and dimensional analysis algorithm for the prediction of mechanical properties of bulk materials and thin films. *Surf. Coat. Technol.* **205**, 1386–1392 (2010).
22. Y.T. Cheng and C.M. Cheng: Scaling, dimensional analysis, and indentation measurements. *Mater. Sci. Eng., R.* **44**, 91–149 (2004).
23. J. Alcalá and D. Esqué-De Los Ojos: Reassessing spherical indentation: Contact regimes and mechanical property extractions. *Int. J. Solids Struct.* **47**, 2714–2732 (2010).
24. M. Mata and J. Alcalá: The role of friction on sharp indentation. *J. Mech. Phys. Solids* **52**, 145 (2004).
25. E. Harsono, S. Swaddiwudhipong, and Z.S. Liu: The effect of friction on indentation test results. *Modell. Simul. Mater. Sci. Eng.* **16**, 065001 (2008).
26. S.A. Rodríguez, M.C. Farias, and R.M. Souza: Analysis of the tip roundness effects on the micro- and macroindentation response of elastic-plastic materials. *J. Mater. Res.* **24**, 1037–1044 (2009).
27. S.A. Rodríguez, M.C. Farias, and R.M. Souza: Analysis of the effects of conical indentation variables on the indentation response of elastic-plastic materials through factorial design of experiment. *J. Mater. Res.* **24**, 1222–1234 (2009).
28. C.E.K. Mady, S.A. Rodríguez, A.G. Gómez, and R.M. Souza: Effects of mechanical properties, residual stress and indenter tip geometry on instrumented indentation data in thin films. *Surf. Coat. Technol.* **205**, 1393–1397 (2010).
29. W.C. Oliver and G.M. Pharr: Measurement of hardness and elastic modulus by instrumented indentation: Advances in understanding and refinements to methodology. *J. Mater. Res.* **19**, 3–20 (2004).
30. Y. Sun, S. Zheng, T. Bell, and J. Smith: Indenter tip radius and load frame compliance calibration using nanoindentation loading curves. *Philos. Mag. Lett.* **79**, 649–658 (1999).
31. Y.T. Cheng and C.M. Cheng: Relationships between hardness, elastic modulus, and the work of indentation. *Appl. Phys. Lett.* **73**, 614–616 (1998).
32. Y.P. Cao, X.Q. Qian, J. Lu, and Z.H. Yao: An energy-based method to extract plastic properties of metal materials from conical indentation tests. *J. Mater. Res.* **20**, 1194–1206 (2005).
33. R.B. King: Elastic analysis of some punch problems for a layered medium. *Int. J. Solids Struct.* **23**, 1657–1664 (1987).
34. S.A. Rodríguez: Modelamento do Ensaio de Indentação Instrumentada Usando Elementos Finitos e Análise Dimensional– Análise de Unicidade, Variações Experimentais, Atrito e Geometria e Deformações do Indentador. Ph.D. Thesis, University of São Paulo, São Paulo, Brazil, 2010.
35. O. Casals, J. Ocenasek, and J. Alcalá: Crystal plasticity finite element simulations of pyramidal indentation in copper single crystals. *Acta Mater.* **55**, 55–68 (2007).
36. J. Alcalá, D. Esque-De Los Ojos, and S.A. Rodríguez: The role of crystalline anisotropy in mechanical property extractions through Berkovich indentation. *J. Mater. Res.* **24**, 1235–1244 (2009).
37. S.A. Rodríguez, J. Alcalá, and R.M. Souza: Effects of elastic indenter deformation on spherical instrumented indentation tests: The reduced elastic modulus. *Philos. Mag.* **91**, 7–9 (2010).
38. M. Mata and J. Alcalá: Mechanical property evaluation through sharp indentations in elastoplastic and fully plastic contact regimes. *J. Mater. Res.* **18**, 1705–1709 (2003).
39. O. Casals, J. Alcalá, and J. Očenášek: Micromechanics of pyramidal indentation in fcc metals: Single crystal plasticity finite element analysis. *J. Mech. Phys. Solids* **56**, 3277–3303 (2008).
40. N.A. Sakharova, J.V. Fernandes, J.M. Antunes, and M.C. Oliveira: Comparison between Berkovich, Vickers and conical indentation tests: A three-dimensional numerical simulation study. *Int. J. Solids Struct.* **46**, 1095–1104 (2009).
41. S. Swaddiwudhipong, J. Hua, K.K. Tho, and Z.S. Liu: Equivalency of Berkovich and conical load-indentation curves. *Modell. Simul. Mater. Sci. Eng.* **14**, 71–82 (2006).

https://doi.org/10.1557/jmr.2012.164 Published online by Cambridge University Press